Special Collection

Decomposition of Carbonate-Based Electrolytes: Differences and Peculiarities for Liquids vs. Polymers Observed Using Operando Gas Analysis

Christofer Sångeland[+],[a] Bing Sun[+],[b] Daniel Brandell,[a] Erik J. Berg,[b, c] and Jonas Mindemark*[a]

Direct tracking of solid polymer electrolyte (SPE) decomposition in comparison to a liquid analogue was accomplished by monitoring the evolution of volatile species using online electrochemical mass spectrometry (OEMS). Reduction of a poly (trimethylene carbonate)-based SPE was dominated by CO_2 formation. Detection of CO_2 and an absence of CO confirms a preferred reduction degradation pathway involving C–O bond cleavage at the carbonyl carbon, in correlation with earlier suggestions. In contrast, the alkyl carbonate-based liquid electrolyte exhibited extensive ethylene formation. Trace quantities of H_2 evolution ascribed to water impurities were also observed in both systems. During oxidation, the SPE and liquid electrolyte exhibited CO_2, CO and SO_2 evolution synonymous with electrolyte solvent and salt degradation, albeit at different potentials. Overall, gas evolution rates and redox currents were lower in the SPE system. OEMS revealed significant gas formation independent of current response, as such highlighting the limitations of the voltammetry technique commonly used today to assess electrochemical stability.

1. Introduction

Despite the rapid advances in high-energy and high-power electrode materials for the next generation of lithium-ion batteries (LIBs), electrolyte systems which are intrinsically safe and capable to support long-term stable cell performance remain insufficiently developed.[1] Conventional liquid electrolytes still dominate commercial systems,[2] but their practical application has been continuously challenged by the risks of thermal runaway, their intrinsic flammability and the evolution of hazardous gases which stem from electrolyte decomposition.[3] Hence, from a practical standpoint, electrolytes which are capable of simultaneously fulfilling several criteria – e.g., chemical inertness, wide electrochemical stability window, fast Li^+ transport within a broad temperature range, non-toxicity, non-flammability, cost-effectiveness, minimal ecological footprint from cradle-to-grave and mass-scalability – are in high demand.[4] In this regard, all-solid-state LIBs and Li-metal batteries (LMBs) using solid polymer electrolytes (SPEs) are drawing much interest for safety-critical applications.[5] Given a relatively simple electrolyte formulation consisting of a polymer host material (e.g. high-molecular-weight polyether) doped with a Li-salt, e.g. lithium bis(trifluoromethanesulfonyl)imide (LiTFSI) or lithium bis(fluorosulfonyl)imide (LiFSI),[6] SPEs have been particularly attractive, credited to their chemical robustness and mechanical stability. Nevertheless, a major challenge for conventional polyether-based SPEs has been the limited ionic conductivity at ambient temperature (typically on the order of $\sim 10^{-7}$ S cm^{-1} at room temperature) and low cation transference number ($T_+ < 0.2$),[7] although recent progress in SPEs based on alternative ion-coordinating moieties (e.g., polycarbonates and polyesters) has shown improved electrolyte properties at ambient temperature,[6,8] which opens up new opportunities for SPE implementation.

Fast ion transport is not the sole critical parameter that influences cell performance; for liquid electrolytes it is well known that the stability of the electrolyte plays an integral role in the capacity retention and cell durability of LIBs,[3b,9] and solid-state electrolytes are no exception. Non-passivating solid electrolyte interphase (SEI) and cathode electrolyte interphase (CEI) growth leads to continuous cell impedance increase and loss of lithium inventory. Despite its importance, there remains a large knowledge gap regarding the interfacial stability in solid-state batteries, in contrast to the prominent research on

[a] C. Sångeland,[+] Prof. D. Brandell, Dr. J. Mindemark
Department of Chemistry – Ångström Laboratory
Uppsala University
751 21 Uppsala, Sweden
E-mail: Jonas.mindemark@kemi.uu.se
[b] Dr. B. Sun,[+] Dr. E. J. Berg
Electrochemical Energy Storage Section,
Electrochemistry Laboratory
Paul Scherrer Institute
5232 Villigen PSI, Switzerland
[c] Dr. E. J. Berg
Present address:
Department of Chemistry – Ångström Laboratory
Uppsala University
751 21 Uppsala, Sweden
[+] These authors contributed equally to this work.

Supporting information for this article is available on the WWW under https://doi.org/10.1002/batt.202000307

Special Collection An invited contribution to a joint Special Collection between Batteries & Supercaps and Chemistry-Methods on In Situ and Operando Methods for Energy Storage and Conversion

liquid electrolytes. Analogous to liquid electrolytes, SPEs are expected to decompose when subjected to potentials that exceed their electrochemical stability window. By voltammetry techniques, the anodic oxidation onsets of poly(ethylene oxide)- and polycarbonate-based SPEs have been estimated to 4.0–4.5 V vs. Li^+/Li.[8a,10] In graphite half-cells, SPEs exhibited no clear plateau indicative of SEI formation during the initial charge cycle at 0.8–1.0 V vs. Li^+/Li, which is otherwise seen in alkyl carbonate-based liquid electrolytes.[11] Given the challenging sample preparation for post-mortem analysis of SPE/electrode interfaces,[12] there are notably few studies depicting the formation and composition of interphase layers in solid-state batteries.[13] Questions still remain about the true stability of SPEs, what role impurities play, what decomposition species may evolve at the interfaces, and how these species impact the performance of solid-state LIBs. Furthermore, the effect of elevated operating temperature – which has proven detrimental to LIB longevity and require additional thermal sensors and cooling systems – has yet to be investigated in LIBs with SPEs.[14] To this end, the development of new *in situ* techniques can offer insight into electrolyte degradation in solid-state batteries, similar to what has been achieved in the field of liquid electrolytes.[15] Online Electrochemical Mass Spectrometry (OEMS) has proved to be an effective tool to monitor the decomposition reactions of liquid alkyl carbonates by tracking time- and potential-dependent evolution of gaseous products.[16] For instance, OEMS has shown that the reduction of ethylene carbonate yielded H_2 and C_2H_4 gas release.[16a,17] Autocatalytic reactions stemming from $LiPF_6$ salt (e.g., POF_3 formation) and cell impurities have also been observed.[16a,18] To this end, we have implemented OEMS to gain further understanding of the formation of key SEI and CEI components in a polycarbonate-based solid polymer electrolyte system previously identified using post mortem XPS.[12]

2. Results and Discussion

As a first attempt to use OEMS to depict SPE degradation, a custom-made two-electrode cell OEMS setup[19] (see Figure 1) was implemented in this study to monitor the evolution of volatile species during the electrochemical reduction and oxidation of a polymer electrolyte consisting of poly (trimethylene carbonate) (PTMC) and LiTFSI salt. PTMC:LiTFSI was specifically selected as a solid analogue to a carbonate-based liquid electrolyte consisting of ethylene carbonate (EC), diethyl carbonate (DEC) and LiTFSI. PTMC and its cyclic monomer trimethylene carbonate (TMC) closely resemble the constituents of EC/DEC which provides a compelling comparison between degradation of SPEs and organic liquid electrolytes. From a practical standpoint, an advantage of the SPE is its non-volatility, which means that the electrolyte in the OEMS does not dry out over time.

The gas evolution profiles of PTMC + 25 wt% LiTFSI and 1 M LiTFSI in EC:DEC (3:7 w/w) recorded during reduction and oxidation can be seen in Figure 2 and 3, respectively. Details regarding gas identification can be found in the experimental

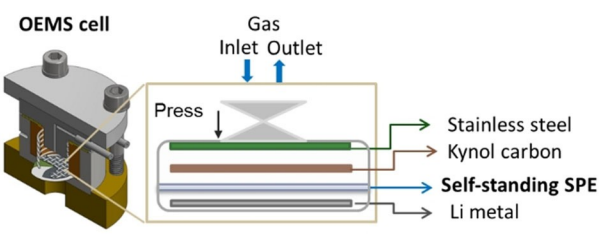

Figure 1. A schematic illustration of the OEMS cell used to analyze the volatile species during reduction and oxidation of the SPE.

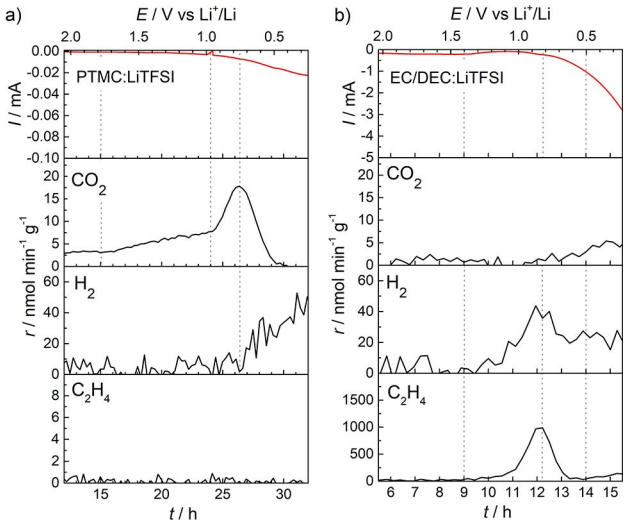

Figure 2. CO_2 ($m/z = 44$), H_2 ($m/z = 2$) and C_2H_4 ($m/z = 27$) gas evolution profiles of (a) 25 wt% LiTFSI in PTMC; (b) 1 M LiTFSI in EC:DEC (3:7 w/w) within 2.0–0 V vs. Li^+/Li.

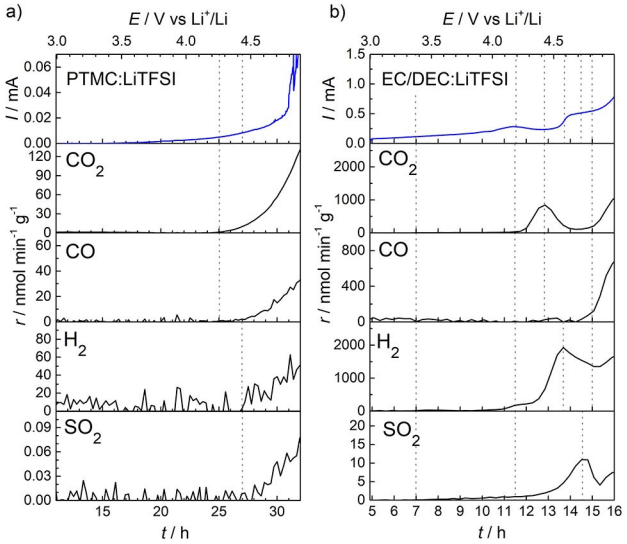

Figure 3. CO_2 ($m/z = 44$), CO ($m/z = 28$*), H_2 ($m/z = 2$) and SO_2 ($m/z = 64$) gas evolution profiles of (a) 1 M LiTFSI in EC/DEC; (b) 25 wt% LiTFSI in PTMC within 3.0–5.0 V vs. Li^+/Li. Mass traces belonging to CO were estimated by subtracting 14% of the $m/z = 44$ signal contribution from the total $m/z = 28$ signal to account for $m/z = 28$ fragments originating from CO_2.

section. As seen in Figure 2a, noticeable reduction as evidenced by gas formation began at approximately 1.75 V vs. Li^+/Li for PTMC:LiTFSI, while EC/DEC:LiTFSI exhibited a reduction onset at 1.4 V. Overall, reduction currents observed in the liquid electrolyte system were two orders of magnitude larger than in the SPE system. This is expected despite the lower measurement temperature (room temperature vs. 50 °C) partly because EC/DEC:LiTFSI exhibits better wetting properties and hence the electrolyte–electrode contact area is significantly larger, but also because the solid PTMC:LiTFSI membrane can limit the flux of species towards and away from the electrode. Interestingly, the gas formation profiles in both systems shares little resemblance with the current response, hence highlighting the limitations of linear sweep voltammetry (LSV) to determine the true electrochemical stability.

The onset of reduction current in PTMC:LiTFSI is marked by CO_2 formation. The rate of CO_2 evolution increased further at roughly 1.0 V indicating the beginning of a secondary electrolyte degradation process, before peaking at 0.75 V and then dying off and reaching nominal levels at 0.5 V. EC/DEC:LiTFSI hardly displayed any CO_2 formation, possibly only minor amounts at a later stage <0.8 V. Instead, C_2H_4 was detected below 1.4 V and the evolution rate continued to rise until the peak at 0.8 V followed by a decrease back down until 0.65 V. Previous experimental and computational studies on the reduction of alkyl carbonate solvents confirm these observations and also offer an explanation to their origin.[18,20] Cyclic and linear carbonate solvents can be chemically decomposed to CO_2 in a nucleophilic attack by strong Lewis bases (e.g. OH^-, alkoxides) generated during electrolyte reduction.[20a,b] Ethylene formation is typically observed in EC-containing electrolytes undergoing two-electron reduction during SEI formation. Alkanes have been exclusively detected from linear carbonates (e.g., DEC).[20b,21]

From post-mortem studies on PTMC:LiTFSI graphite half-cells, two decomposition pathways were previously proposed, one involving CO_2 formation and the other CO formation.[12] The detected CO_2 and the absence of CO (see Figure S1) in the present work evidences the decomposition pathways during PTMC:LiTFSI reduction proposed in Figure 4a. This confirms recent computational work indicating that the $C_{ethereal}$—$O_{ethereal}$ bond is energetically more prone to breakage compared to the $C_{carbonyl}$—$O_{ethereal}$ bond in PTMC under strongly reducing conditions.[22] Similarly to EC, additional CO_2 may also be generated from the reduction of residual TMC monomers[23] (concentration previously estimated to be <7 ‰);[8a] however, the distinctive broad hump at 2.9–2.1 V during reduction of the monomer (Figure S2) is not observed in Figure 2, indicating negligible contribution from TMC monomer residues.

Other than CO_2 and C_2H_4, both EC/DEC:LiTFSI and PTMC:LiTFSI exhibited H_2 formation of similar magnitude during reduction, albeit at low concentrations. EC/DEC:LiTFSI exhibited an increase in H_2 generation rate at 1.4 V before peaking at 0.8 V and then leveling off. In comparison, hydrogen evolution in PTMC:LiTFSI began much later at 0.75 V and continued to increase steadily. Previous research ascribed H_2 release to reduction of water impurities in alkyl carbonate

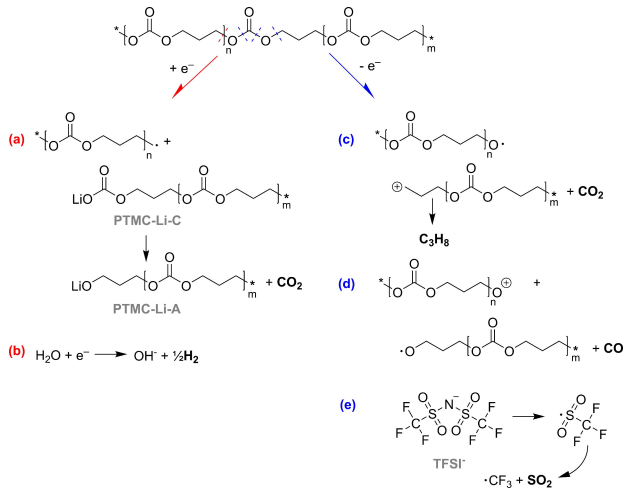

Figure 4. Schematic illustrations of possible decomposition pathways during reduction (a–b) and oxidation (c–f) of PTMC:LiTFSI. Gases detected using OEMS are highlighted in bold.

electrolytes;[16b,17a,24] the deliberate addition of water (up to 4000 ppm) to LiTFSI-containing electrolytes resulted in accelerated H_2 evolution from graphite half-cells below 1.6 V vs. Li^+/Li.[25] Upon reduction of 'free water' in EC-based electrolytes, hydroxide ions are also formed, which can induce hydrolysis of EC molecules and subsequently cause ring-opening followed by H_2 and CO_2 formation.[20a,26] The recorded CO_2 and H_2 gas profiles for EC/DEC:LiTFSI exhibits behavior synonymous with water reduction. In the case of PTMC electrolytes, low concentrations of water impurities (below approximately 40 ppm) have been observed even though the polymer component is relatively hydrophobic.[12] Assuming a single-electron reduction,[21] 1 mol of H_2O would generate 0.5 mol of H_2, a PTMC sample (thickness 100 μm, diameter 22 mm) would generate approximately 0.04 μmol of H_2, which is close to the total amount of H_2 detected (approximately 0.05 μmol). Another argument in favor of water reduction taking place in PTMC:LiTFSI is the rapid decline of CO_2 following the onset of H_2 seen in Figure 2, which can be explained by a secondary reaction between CO_2 and OH^- to form HCO_3^- and then Li_2CO_3,[25–26] a common SEI species in SPEs with water impurities.[11] OH^- can also attack polymer chains resulting in a metastable mono-substituted carboxyl group that can undergo further fragmentation and form CO_2 and an alcohol. The discrepancy between the observed onset of H_2 evolution in PTMC:LiTFSI (0.75 V vs. Li^+/Li) compared to the onset observed for EC/DEC:LiTFSI (1.4 V) and the onset reported for EC/DEC:LiTFSI and EC/DEC:$LiPF_6$ (1.6 and 1.8 V, respectively),[25,27] can be explained by the liquid electrolyte reaching contact with the stainless steel mesh beneath the kynol electrode, unlike the restricted solid diffusion of SPE which only allows contact to the kynol electrode and not the stainless steel. Metal surfaces have a higher electrocatalytic activity for hydrogen evolution reactions in comparison to carbon surfaces and can thus explain the observed difference in H_2 evolution onset.[28]

Gas evolution during oxidation to 5 V vs. Li^+/Li was also monitored, see Figure 3. PTMC:LiTFSI began oxidizing at

approximately 3.8 V and the current continued to rise steadily until 4.6 V, after which the oxidation current rapidly increased, see Figure 3a. Potential-dependent CO_2 generation began at 4.25 V and continued until the upper potential limit. The erratic current behavior at above 4.6 V was not echoed in the gas profiles, which indicates alternative non-gaseous degradation reactions at higher potentials. CO_2 evolution was also reported for poly(propylene carbonate):LiTFSI, but at 3.5 V vs. Li^+/Li followed by an increase at 4 V,[29] albeit with a working electrode consisting of the active material $LiFePO_4$. In addition to CO_2, minor traces of $m/z=43$ were observed, see Figure S3a, which may indicate propane release during breakdown of TMC repeating units, see Figure 4c. From this material, C_2 fragments are unlikely to be generated and the absence of fragments at $m/z=27$ indeed rules out the formation of ethylene. Once again, we observe little contribution from the oxidation of TMC monomer residues since the distinctive twin peaks at 3.8 and 4.0 V in the oxidation profile seen in Figure S2 are not present in Figure 3a. Lastly, H_2 evolution was observed at 4.4 V, which most likely stems from oxidation of the polymer followed by subsequent 'crosstalk' of H^+ ions and reduction at the anode.[16b]

In comparison to the SPE, EC/DEC:LiTFSI exhibited noticeable oxidation at approximately 3.4 V vs. Li^+/Li, with peaks appearing at 4.2 and 4.6 V, see Figure 3b. Between 3.4 and 4.1 V, OEMS detected minor traces of CO in correlation with an increasing oxidation current. Coinciding with the oxidation peak at 4.2 V, there was a local maximum for H_2 formation and the early onset of CO_2 formation as a result of ring-opening of EC accompanied by CO_2 release and proton abstraction followed by H^+ 'cross talk' and H_2 evolution.[16b] Interactions of neighboring EC complexes might further result in nucleophilic attack through the carbonyl groups, releasing CO_2 and possibly aldehyde.[20c] Mass traces typically associated with aldehyde fragments[30] or ethyl groups from DEC ($m/z=29$) were detected at low anodic potentials close to 3.4 V (Figure S3b); however, aldehyde traces could also be attributed to the functional groups on the Kynol carbon cloth substrate.[19] Additional secondary reactions like deprotonation could also be triggered by anion nucleophilic attack of anion–solvent complexes (e.g., EC–TFSI) on carbonate solvents upon electron removal.[20d] Remaining $m/z=16$ fragments not accounted to CO_2 were also detected, possibly methane (Figure S3). Following the onset at 4.2 V, the rate of CO_2 generation continued to increase until 4.4 V, after which it subsided to initial levels. At approximately 4.8 V, CO_2 as well as CO began to rapidly increase, attributed to high-voltage oxidation of EC.[16b,31]

Notably, SO_2 evolution ($m/z=64$) at higher oxidation potentials was observed in both PTMC:LiTFSI and EC/DEC:LiTFSI, see Figure 3. The origin of SO_2 can be explained by the breakage of the relatively weak N–S bond in the TFSI anions. Subsequent CF_3–$SO_2^\bullet$ radicals may undergo further cleavage to form $CF_3^\bullet$ and SO_2, see Figure 4e.[32] The onset of SO_2 formation observed at approximately 4.4 V and 4.2 V vs. Li^+/Li in PTMC:LiTFSI and EC/DEC:LiTFSI, respectively, could be assigned to salt decomposition. Solid salt residues (e.g., LiF, Li_2S, Li_2SO_3) on cathode surfaces in both liquid electrolytes and PTMC-based SPEs have also been reported.[12,33] Interestingly, the formation of SO_2 occurs at a much higher potential compared to formation of solid products reported by *ex situ* X-ray photoelectron spectroscopy of the interface between PTMC:LiTFSI and $LiFePO_4$, possibly indicating either gas evolution post-CEI formation or catalytic effects of the $LiFePO_4$ electrode material.[12] Following oxidation, salt-derived radicals or trace oxygen radicals can attack the polymer chains and initiate secondary reactions.[32b] It has also been suggested that TFSI anions could attack the polymer chains and initiate other secondary reactions, e.g., hydrogen abstraction accompanied by H_2 release.[34] This raises the question of which component of the SPE that determines the upper limit of the electrochemical stability window; the salt, the polymer host, or the impurities? Based on computational modelling, we know that the electrochemical stability varies significantly when looking at the polymer and salt separately compared to the combination of the two.[35] Hence, we would like to stress the importance of studying these materials in their entirety and not as individual components. Degradation is not necessarily undesirable; for instance, inserting a thin artificial layer of LiF proved to effectively prevent oxidation of the PPC:LiTFSI SPE and hence also over-charging,[29] thus demonstrating the positive role of salt degradation species in the CEI. Compared to the SPE system, the liquid electrolyte exhibited exaggerated gas evolution (two orders of magnitude larger), likely a result of improved ion transfer and surface contacts at the liquid electrolyte/electrode interface. Unlike the relatively rapid growth of interphase layers in liquid electrolytes, it is expected that SPE/electrode interfaces are relatively stationary and stable over time. In the absence of convection, the decomposition reactions are likely occurring solely within a thin layer, with a minimal tendency to propagate through the bulk SPE.

3. Conclusions

Understanding solid electrolyte interphase formation and its practical implications for battery performance beyond the known context of idealized systems and electrochemical stability windows is the next challenging step towards realizing high-performance all-solid-state batteries. In this work, potential-dependent gas evolution during reduction and oxidation provides direct evidence of polymer electrolyte decomposition. The significantly lower redox currents and gas traces from the polycarbonate-based SPE offer the potential option of suppression of cell gassing using SPEs in relevant battery applications. In the case of the SPE, the presence of CO_2 and absence of CO during reduction confirmed a degradation pathway previously proposed from post-mortem and computational studies. It is also evident that small amounts of electrolyte impurities such as residual water actively participate in the degradation process. Finally, OEMS detected gas formation which was not evident in the voltammetry sweeps thus highlighting the limitations of traditional voltammetry techniques to determine electrochemical stability limits. With these findings we have shown that the electrochemical degradation of polycarbonate-

based SPEs and liquid alkyl carbonate solvents share many similarities but also differ in terms of evolution of volatile species. Hence, we believe that common understanding of effective SEI and CEI formation in liquid electrolytes cannot be directly applied to SPE systems, thereby opening up for renewed and expanded discourses.

Experimental Section

Polymer electrolyte sample preparation

PTMC with a molecular weight of 368 000 g mol^{-1} was prepared using bulk-ring polymerization described elsewhere.[8a] The obtained material was dissolved in anhydrous acetonitrile (Sigma Aldrich) along with LiTFSI salt (Purolyte, dried at 120 °C for 48 h under vacuum). The concentration of LiTFSI salt was 25 wt% and was selected based on the optimal ionic conductivity for the PTMC:LiTFSI system.[8a] Finally, self-standing SPE films were obtained by evaporating the solvent using a vacuum oven.[36]

Electrochemical characterization of TMC monomer

The electrochemical response of TMC:LiTFSI was determined by linear sweep voltammetry (LSV) at 50 °C with a scan rate of 0.025 mV s^{-1} using a Bio-Logic VMP2. The cell configuration was Li | TMC with 20 wt% LiTFSI and glass fiber separator | carbon cloth (Kynol, ACC-507-20). Separate LSV measurements from 3.0–0 V and 3.0–5.0 V vs. Li$^+$/Li were done to determine the anodic and cathodic response.

Online electrochemical mass spectrometry

A custom-made two-electrode cell setup[19] adapted for SPE films was used for all OEMS measurements, see Figure 1. High-surface-area carbon cloth (Kynol, ACC-507-20), mechanically supported by a stainless steel current collector, was chosen as the working electrode in order to amplify the evolved gas quantities and promote surface contacts at the electrode/SPE interface. A thin Li foil (Rockwood Lithium), 20 mm in diameter and 0.22 mm in thickness, was used as the counter and reference electrode. Reduction and oxidation measurements on PTMC:LiTFSI SPE films were done from 3.0–0 V and 3.0–5.0 V vs. Li$^+$/Li with a scan rate of 0.025 mV s^{-1} at 50 ± 1 °C. Measurements on the liquid electrolyte analogue, 1 M LiTFSI in EC/DEC (3:7 w/w), were done at room temperature at 0.05 mV s^{-1}. Measurement temperatures and sweep rates were based on typical operating conditions for liquid and solid-state polymer electrolyte systems. Despite comparing the systems at different temperatures, no differences in gas formation onset potential or which types of gases are evolved is expected, only larger quantities at higher temperatures.[37] Evolved gases were continuously traced from the head space of OEMS cells by a controlled Ar flow to the inlet of a quadrupole mass spectrometer (MS, QMS200, Pfeiffer). The partial pressure of gas species in Ar flow was documented as MS ion-current intensity and then converted to evolution rate (μmol min^{-1}) and then normalized according to the mass of the working electrode (μmol min^{-1} g^{-1}). The amount of evolved gases – H_2 ($m/z = 2$), CH_4 ($m/z = 16$), C_2H_4 ($m/z = 27$), and CO_2 ($m/z = 44$) – were quantified and calibrated with standard calibration gases: 0.1 mol% C_2H_4, 0.1 mol% CH_4, and 0.1 mol% CO_2 in Ar 5.0 gas (Messer, Switzerland). Signals arising from CO_2 overlap CO, hence, the amount of CO ($m/z = 28$*) was estimated by subtracting the fragment contribution of CO_2, see the equation below [Eq. (1)]:

$$I_{28}* = I_{28} - 0.14 \times I_{44} \quad (1)$$

The fragmentation of the different gas molecules can be seen in Table S1.

Acknowledgements

C.S., D.B., and J.M. acknowledge STandUP for Energy, Batteries Sweden (BASE) and ECO^{2}LIB (European Union H2020 research and innovation programme under Grant agreement No 875514) for financial support. B.S. and E.J.B. acknowledge the Swiss national Science Foundation (SNSF) under the "Ambizione Energy" funding scheme (Grant 160540).

Conflict of Interest

The authors declare no conflict of interest.

Keywords: electrochemical stability window · gas evolution · online electrochemical mass spectrometry · solid-state electrolytes · solid polymer electrolytes

[1] K. Xu, *Chem. Rev.* **2014**, *114*, 11503–11618.
[2] D. Aurbach, Y. Talyosef, B. Markovsky, E. Markevich, E. Zinigrad, L. Asraf, J. S. Gnanaraj, H.-J. Kim, *Electrochim. Acta* **2004**, *50*, 247–254.
[3] a) E. P. Roth, C. J. Orendorff, *Electrochem. Soc. Interface* **2012**, *21*, 45–49; b) H. J. Peng, S. Urbonaite, C. Villevieille, H. Wolf, K. Leitner, P. Novák, *J. Electrochem. Soc.* **2015**, *162*, A7072–A7077.
[4] D. Larcher, J. M. Tarascon, *Nat. Chem.* **2015**, *7*, 19–29.
[5] J. Nair, L. Imholt, G. Brunklaus, M. Winter, *Electrochem. Soc. Interface* **2019**, *28*, 55–61.
[6] J. Mindemark, M. J. Lacey, T. Bowden, D. Brandell, *Prog. Polym. Sci.* **2018**, *81*, 114–143.
[7] D. Devaux, R. Bouchet, D. Glé, R. Denoyel, *Solid State Ionics* **2012**, *227*, 119–127.
[8] a) B. Sun, J. Mindemark, K. Edström, D. Brandell, *Solid State Ionics* **2014**, *262*, 738–742; b) Y. Tominaga, *Polym. J.* **2017**, *49*, 291–299.
[9] a) K. Edström, T. Gustafsson, J. O. Thomas, *Electrochim. Acta* **2004**, *50*, 397–403; b) K. Edström, M. Herstedt, D. P. Abraham, *J. Power Sources* **2006**, *153*, 380–384.
[10] a) W. Xu, J.-P. Belieres, C. A. Angell, *Chem. Mater.* **2001**, *13*, 575–580; b) J. Mindemark, B. Sun, E. Törmä, D. Brandell, *J. Power Sources* **2015**, *298*, 166–170; c) Y.-C. Jung, M.-S. Park, D.-H. Kim, M. Ue, A. Eftekhari, D.-W. Kim, *Sci. Rep.* **2017**, *7*, 17482–17492.
[11] C. Xu, B. Sun, T. Gustafsson, K. Edström, D. Brandell, M. Hahlin, *J. Mater. Chem. A* **2014**, *2*, 7256–7264.
[12] B. Sun, C. Xu, J. Mindemark, T. Gustafsson, K. Edström, D. Brandell, *J. Mater. Chem. A* **2015**, *3*, 13994–14000.
[13] C. Sångeland, J. Mindemark, R. Younesi, D. Brandell, *Solid State Ionics* **2019**, *343*, 115068–115081.
[14] S. Ma, M. Jiang, P. Tao, C. Song, J. Wu, J. Wang, T. Deng, W. Shang, *Prog. Nat. Sci.* **2018**, *28*, 653–666.
[15] a) C. P. Grey, J. M. Tarascon, *Nat. Mater.* **2017**, *16*, 45–56; b) T. Minato, T. Abe, *Prog. Surf. Sci.* **2017**, *92*, 240–280.
[16] a) A. Guéguen, D. Streich, M. He, M. Mendez, F. F. Chesneau, P. Novák, E. J. Berg, *J. Electrochem. Soc.* **2016**, *163*, A1095–A1100; b) M. Metzger, B. Strehle, S. Solchenbach, H. A. Gasteiger, *J. Electrochem. Soc.* **2016**, *163*, A798–A809; c) D. Streich, A. Guéguen, M. Mendez, F. Chesneau, P. Novák, E. J. Berg, *J. Electrochem. Soc.* **2016**, *163*, A964–A970; d) M. Moshkovich, M. Cojocaru, H. E. Gottlieb, D. Aurbach, *J. Electroanal. Chem.* **2001**, *497*, 84–96.
[17] a) R. Imhof, P. Novák, *J. Electrochem. Soc.* **1998**, *145*, 1081–1087; b) D. M. Seo, D. Chalasani, B. S. Parimalam, R. Kadam, M. Nie, B. L. Lucht, *ECS Electrochem. Lett.* **2014**, *3*, A91–A93; c) X. Teng, C. Zhan, Y. Bai, L. Ma, Q.

Liu, C. Wu, F. Wu, Y. Yang, J. Lu, K. Amine, *ACS Appl. Mater. Interfaces* **2015**, *7*, 22751–22755.
[18] X. Zhang, R. Kostecki, T. J. Richardson, J. K. Pugh, P. N. Ross, *J. Electrochem. Soc.* **2001**, *148*, A1341–A1345.
[19] M. He, *Elucidating interface reactions in Li-ion batteries and supercapacitors by in situ gas analysis*, ETH Zürich **2016**.
[20] a) G. Gachot, S. Grugeon, M. Armand, S. Pilard, P. Guenot, J.-M. Tarascon, S. Laruelle, *J. Power Sources* **2008**, *178*, 409–421; b) M. Onuki, S. Kinoshita, Y. Sakata, M. Yanagidate, Y. Otake, M. Ue, M. Deguchi, *J. Electrochem. Soc.* **2008**, *155*, A794-A797; c) L. Xing, O. Borodin, *Phys. Chem. Chem. Phys.* **2012**, *14*, 12838–12843; d) O. Borodin, W. Behl, T. R. Jow, *J. Phys. Chem. C* **2013**, *117*, 8661–8682.
[21] P. Novák, F. Joho, R. Imhof, J.-C. Panitz, O. Haas, *J. Power Sources* **1999**, *81–82*, 212–216.
[22] M. Ebadi, C. Marchiori, J. Mindemark, D. Brandell, C. M. Araujo, *J. Mater. Chem. A* **2019**, *7*, 8394–8404.
[23] D. Aurbach, *Nonaqueous electrochemistry*, 1 ed., CRC Press, Boca Raton **1999**.
[24] R. Bernhard, M. Metzger, H. A. Gasteiger, *J. Electrochem. Soc.* **2015**, *162*, A1984–A1989.
[25] P. G. Kitz, P. Novák, E. J. Berg, *ACS Appl. Mater. Interfaces* **2020**, *12*, 15934–15942.
[26] M. Metzger, B. Strehle, S. Solchenbach, H. A. Gasteiger, *J. Electrochem. Soc.* **2016**, *163*, A1219–A1225.
[27] N. Mozhzhukhina, E. Flores, R. Lundström, V. Nyström, P. G. Kitz, K. Edström, E. J. Berg, *J. Phys. Chem. Lett.* **2020**, *11*, 4119–4123.
[28] R. Koutavarapu, C. Venkata Reddy, B. Babu, K. R. Reddy, M. Cho, J. Shim, *Int. J. Hydrogen Energy* **2020**, *45*, 7716–7740.
[29] J. Li, S. Dong, C. Wang, Z. Hu, Z. Zhang, H. Zhang, G. Cui, *J. Mater. Chem. A* **2018**, *6*, 11846–11852.
[30] J. A. Gilpin, F. W. McLafferty, *Anal. Chem.* **1957**, *29*, 990–994.
[31] M. Metzger, C. Marino, J. Sicklinger, D. Haering, H. A. Gasteiger, *J. Electrochem. Soc.* **2015**, *162*, A1123–A1134.
[32] a) C. A. C. Sequeira, J. M. North, A. Hooper, *Solid State Ionics* **1984**, *13*, 175–179; b) F. M. Gray, *Solid Polymer Electrolytes: Fundamentals and Technological Applications*, VCH **1991**.
[33] D. Ensling, M. Stjerndahl, A. Nytén, T. Gustafsson, J. O. Thomas, *J. Mater. Chem.* **2009**, *19*, 82–88.
[34] F. Faglioni, B. V. Merinov, W. A. Goddard, B. Kozinsky, *Phys. Chem. Chem. Phys.* **2018**, *20*, 26098–26104.
[35] C. F. N. Marchiori, R. P. Carvalho, M. Ebadi, D. Brandell, C. M. Araujo, *Chem. Mater.* **2020**, *32*, 7237–7246.
[36] J. Mindemark, E. Törmä, B. Sun, D. Brandell, *Polymer* **2015**, *63*, 91–98.
[37] R. Jung, P. Strobl, F. Maglia, C. Stinner, H. A. Gasteiger, *J. Electrochem. Soc.* **2018**, *165*, A2869–A2879.

Manuscript received: December 3, 2020
Revised manuscript received: December 30, 2020
Version of record online: February 2, 2021